Chapter

Widely Tunable Quantum-Well Laser: OPO Diode Around 2 μm Based on a Coupled Waveguide Heterostructure

Alice Bernard, Jean-Michel Gérard,
Ivan Favero and Giuseppe Leo

Abstract

We present the design of a widely tunable monolithic source on GaAs/AlGaAs. It consists of a quantum-well distributed feedback (DFB) laser vertically coupled with a waveguide engineered for nonlinear frequency conversion. No regrowth or alignment is necessary, and all the structure stems from a single epitaxy step. Light is emitted by the 0.98 μm DFB laser and transmitted to the underlying waveguide by an adiabatic taper, where it can undergo parametric down-conversion, providing signal and idler beams around 2 μm. Transfer rates and tolerances for transfer and conversion efficiency are calculated to be compatible with the tolerances of current fabrication processes. We estimate that an OPO threshold can be reached in the underlying waveguide for a laser emitted power of 20–100 mW, if high-reflectivity distributed Bragg reflectors (DBRs) are used.

Keywords: quantum well, laser diode, near infrared, AlGaAs, tunable source, optical parametric oscillator (OPO), active-passive integration, adiabatic coupling, vertical coupling

1. Introduction

Five decades after the first demonstrations of a laser diode [1, 2], current integrated laser sources include diodes, quantum cascade lasers, and interband cascade lasers. These sources span a wide range from the visible spectrum to the far infrared. However, they present to this day a limited tunability, up to a few tens of nm at the most excluding external cavity setups. This is a limitation in particular in the field of spectroscopy, in demand of coherent and widely tunable sources. In parallel to the development of integrated lasers, optical parametric oscillators (OPOs) have undergone a wide progress, spanning the electromagnetic spectrum from ultraviolet to infrared and providing largely tunable outputs, but they are not yet widely adopted on integrated platforms. This is mostly due to the difficulty of adjusting the phase mismatch in situ and historically to the lack of nonlinear materials in semiconductor platforms. However, GaAs/AlGaAs provides high nonlinear conversion efficiencies, and fabrication efforts have resulted in a diminution of losses in this material system [3, 4]. Optically, pumped OPOs have been demonstrated

IntechOpen

in micrometric GaAs/AlGaAs waveguides through orientation patterning [5] and artificial birefringence [6].

In addition to providing high nonlinear conversion efficiencies, AlGaAs are also a mature platform for laser diodes. As a consequence, a few proposals of all-in-one laser diode/OPO have been made [7, 8], without experimental demonstration to this day. In these proposals, the laser and OPO cavity are one and the same. This configuration reduces fabrication complexity and allows one to harness high intracavity fields. However, the best design parameters for efficient laser behavior tend to degrade nonlinear light conversion and vice versa. More precisely, the main bottleneck in this case is related to the dopant-induced FCA propagation losses. Indeed, in order to achieve an efficient electric injection in the laser, the dopant concentration should be high in the cladding layers. But this introduces FCA losses for the signal and idler beams, hence reducing the conversion efficiency and generated power. As a result, dopant-induced losses are an obstacle to reach the OPO threshold. Another limitation of this configuration is the adjustment of phase mismatch, as the only available in situ tool is temperature, which may degrade laser efficiency if high temperatures are needed.

The main alternative to this approach is heterogeneous integration, a cumbersome and time-intensive method. We propose here an original approach where laser and OPO cavities are distinct but grown on the same wafer. No subsequent alignment or epitaxy regrowth is necessary. This device is based on vertical coupling: laser and OPO cavities are grown on vertically separated layers and coupled so that light can pass from one to the other. Vertical couplers have been widely described for the integration of lasers or detectors on an underlying chip [9]. At the upper level, a material of smaller gap is used for light generation or detection, while the lower levels comprise a material of higher gap for light transmission and analysis. This scheme is also used for the integration of III–V laser on silicon chips [10]. Both systems are analogous to our proposal: a laser is coupled to another waveguide, which provides a secondary function (light modulation, transmission, or in our case conversion). Here, however, design is not straightforward since the fundamental laser mode needs to be coupled to a higher order mode in the underlying waveguide. The use of this higher order mode enables modal phase matching in the buried waveguide, which is optimized for parametric conversion.

We base our design on the growth sheet of a 0.98-μm AlGaAs laser and engineer the OPO cavity to provide down-conversion toward a signal/idler range between 1.8 and 2.2 μm. We rely on modal phase matching between a TE-polarized higher order mode at the pump wavelength and fundamental cross polarized modes at signal/idler wavelengths. As a consequence, the fundamental mode in the laser cavity is transferred to a higher order mode in the OPO cavity. In situ adjustment of the phase mismatch can be achieved through modifications of laser wavelength and temperature of the OPO cavity.

2. General description of the device

In order to provide the best fabrication tolerance, we base our design on an adiabatic taper (instead of, e.g., a resonant coupler that would provide a shorter transfer length). Before detailing the device, we single out here some points critical to its operation. These aspects dictate design choices for the rest of the device.

The first "hard point" is spectral stability. To achieve a lower OPO threshold, we choose a doubly resonant OPO (DR-OPO) configuration. Concerning the laser, to avoid mode competition and instability, the pump should not return into the laser cavity after having explored the OPO region. This requires DBR with

DOI: http://dx.doi.org/ 10.5772/intechopen.80517

high reflectivities at signal/idler wavelengths and low reflectivities at the pump wavelength, as present, for example, in [6]. Furthermore, stability of the device is improved by in situ control of the phase mismatch, through shift of the pump wavelength or of the OPO cavity temperature. These two factors can be tuned independently if the laser and OPO temperatures are set separately. This is possible if the two areas are separated by at least 100 μm and are controlled by individual heaters.

Thermal behavior and contact geometry are also expected to be critical. III/V on Si laser typically emits powers in the 10 mW range [11], while the pump power for OPO threshold is a few tens of mW in our case. The laser should be single mode for stable OPO operation, which imposes a maximal ridge width and thus a minimum optical power density. Furthermore, high-power single-mode lasers are usually shallowly etched (for single-mode operation) and mounted epi-down to limit thermal resistance [12]. In our case, these two aspects cannot be implemented at the same time. Indeed, if the laser is grown on top, the insulating section between laser and doped substrate makes it necessary to use lateral contacts, which requires deep lateral etching and compromises laterally monomode operation. On the opposite, if the laser is grown under the nonlinear (NL) waveguide, shallow etches are possible but epi-down mounting is impossible.

We also carefully examine fabrication tolerances in the region of parametric conversion and assess their impact on conversion efficiency.

2.1 Choice of geometry

To reduce fabrication complexity, we limit ourselves to a single level of etching. This implies that the bottom waveguide geometry is invariant in the direction of propagation and that the top waveguide is narrowed. Keeping in mind the points presented in the previous section, we summarize the advantages of different geometries in **Table 1**. The waveguide where parametric light conversion takes places is called "NL waveguide" (for nonlinear).

We explore the range of possibilities opened by the GaAs/AlAs/InAs system, and we base the design of the laser part on already-existing, high-performance AlGaAs lasers at 1 μm [13]. The detail of layer's thickness and composition is not shown here for confidentiality reasons. In this structure, the fundamental mode at 0.98 μm has an effective index of about 3.36. Regarding the waveguide where parametric conversion is to take place, modal phase matching is more readily achieved if the pump mode is of order 2 in the vertical direction. Additionally, high conversion efficiency is favored by high cladding/core index contrasts. This, coupled with the fact that we have to work with a higher order mode, sets the maximum value of effective index in the waveguide at approximately 3.2. We therefore choose the "laser on top" geometry for its compatibility with effective indices in our project.

This choice has two important consequences. To keep the underlying waveguide undoped, contact for the bottom part of the laser must be taken laterally instead of under the substrate. This implies that the gain region should be deeply etched to clear access to the contacts. This is obviously at odds with a single-mode laser operation, since the important index contrast between air and semiconductor (in the absence of a regrowth step) will cause the laser to oscillate on several transverse modes, unless it is extremely narrow, which is not desirable given the target optical power. As a solution, we propose to etch deeply only one side of the ridge. Single-mode operation can then be achieved with a contact on one side.

2.2 Proposed design

Given the constraints presented earlier, we propose a general design. A general view of the structure is shown in **Figure 1**. On the left, we choose a DFB cavity for the

	Laser on top	NL waveguide on top
	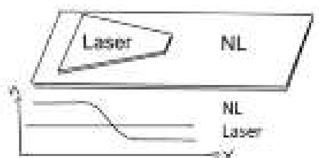	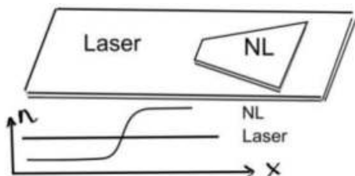
Contacts	Lateral contacts necessary Single-mode operation of the laser is hindered	Lateral contacts not necessary
Thermal control	Epi-up and epi-down possible ☹	Epi-down impossible ☺
Laser multimodality	The laser must start in single-mode operation in a zone in shallow etching; then, it should taper down in the transfer zone (longer total length) 😐	The laser is buried, and single-mode emission is easily achieved ☺
Effective indices	Transition from a high index in the laser to a low index in the NL guide ☺	The laser index should be lower than the indices in the NL waveguide, which are already low (~3.2) ☹

Table 1.
Advantages and drawbacks of different coupling geometries.

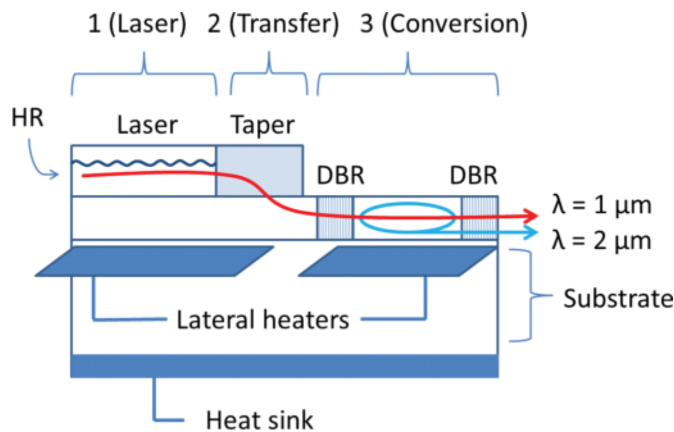

Figure 1.
General view of the proposed coupled-cavity design.

laser in order to provide longitudinal as well as transversal single-mode operation. The upper waveguide narrows in the transfer region, where the mode moves to the bottom waveguide. On the right, parametric conversion takes place in the bottom waveguide, where distributed Bragg reflectors (DBRs) provide a high reflectivity at the signal and idler wavelengths. We will describe the device step-by-step, starting from the end because the zone of parametric conversion is the most sensitive to geometry variations.

2.3 Choice of material

To reach phase matching and a high conversion efficiency, we simulated various waveguide geometries before settling on high index contrasts and a pump of order 2 in the direction of growth. To maximize index contrast in the vertical direction, the waveguide is surrounded by $Al_{0.8}Ga_{0.2}As$ in the bottom cladding and by air above. However, in the region of transfer, the top cladding will be provided by whatever material separates laser and underlying waveguide core. We set this material to be $Al_{0.3}Ga_{0.7}As$, since it is already used as cladding in GaAs lasers. This layer structure is summarized in **Table 2**. It is identical to a standard laser data sheet, apart from the modified separation layer and added nonlinear waveguide and cladding. In the region of frequency conversion, all layers are etched, except for the last three: nonlinear waveguide, bottom cladding, and substrate.

Layer type	Material
Top cladding	AlGaAs
Optical confinement (laser core)	InGaAsP
Quantum well	InGaAs
Optical confinement (laser core)	InGaAsP
Separation layer	$Al_{0.3}Ga_{0.7}As$
Nonlinear waveguide	GaAs
Bottom cladding	$Al_{0.8}Ga_{0.2}As$
Substrate	GaAs

Table 2.
Layer structure proposed for the coupled-cavity design. In the region of conversion, all layers are etched except the last three.

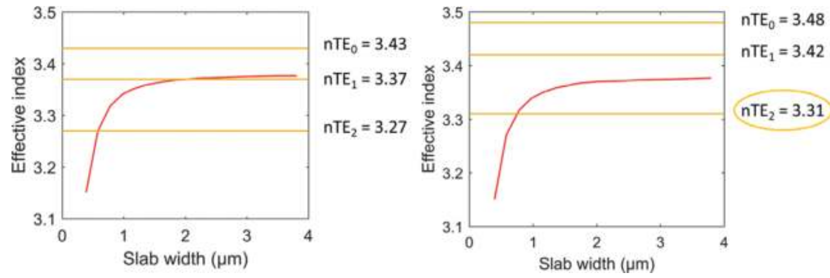

Figure 2.
Effective indices of guided modes in the structure. (Red) Index of the laser mode as a function of guide width. (Orange) Indices of guided modes in the buried waveguide, assuming a planar waveguide of $Al_{0.1}Ga_{0.9}As$ (left) or GaAs (right) surrounded by $Al_{0.3}Ga_{0.7}As$ on one side and $Al_{0.8}Ga_{0.2}As$ on the other.

The waveguide core should hold as little aluminum as possible in order to increase its nonlinear susceptibility. We set the exact Al fraction by comparing the effective index of guided modes in the upper waveguide to the effective index of the lower waveguide as taper width is reduced (**Figure 2**). For 10% Al composition, the laser mode index crosses the index of TE_1 in the buried waveguide. We can thus expect the mode to couple to TE_1. Using pure GaAs, the laser mode crosses only the TE_2 index, which is the desired configuration. Absorption in GaAs at 1 μm is expected to be negligible [14]. Setting a pure GaAs waveguide has another advantage: it eliminates the uncertainty on the Al fraction.

3. Nonlinear characteristics

3.1 Conversion efficiency and OPO threshold

We calculate conversion efficiencies with a code developed in the team, based on the work presented in [15]. **Table 3** shows the nonlinear conversion efficiency at several ridge widths for a waveguide of thickness 0.95 μm surrounded by $Al_{0.8}Ga_{0.2}As$ and air. The corresponding pump powers necessary for an OPO threshold are presented in **Figure 3**. Propagation losses are assumed to be 0.1 cm^{-1}. The threshold pump power lies in the 10–100 mW range.

3.2 Tolerances

Figure 4 shows the SPDC normalized efficiency as a function of ridge width and thickness. The FWHM of efficiency is 200 nm for a variation in width, a value compatible with the current state of fabrication technology. The FWHM for a variation in thickness is much smaller, around 3 nm. The typical precision of thickness achieved by molecular beam epitaxy is approximately 2%, corresponding to a variation of 2 nm in a 0.95 μm waveguide. Depending on growth systems, this value can be further increased by inhomogeneities along the wafer.

Ridge width (μm)	Conversion efficiency (W^{-1} cm^{-2})
2	600
3	380
4	230

Table 3.
SPDC efficiency vs. ridge width in a 0.95-μm-thick waveguide surrounded by $Al_{0.8}Ga_{0.2}As$ and air.

DOI: http://dx.doi.org/ 10.5772/intechopen.80517

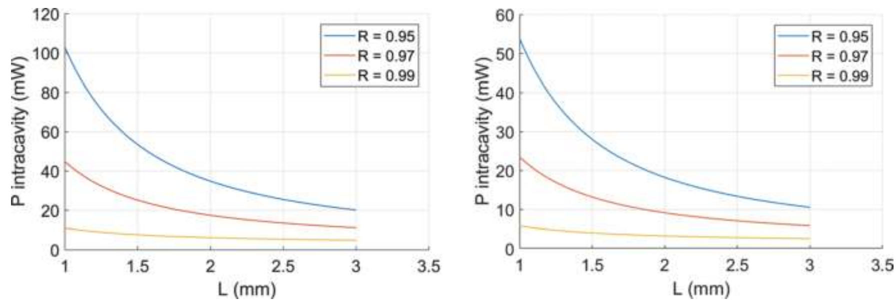

Figure 3.
OPO pump power threshold for a ridge width of 4 μm (left) and 2 μm (right) as a function of length and signal/idler reflectivity. Guide thickness is 0.95 μm.

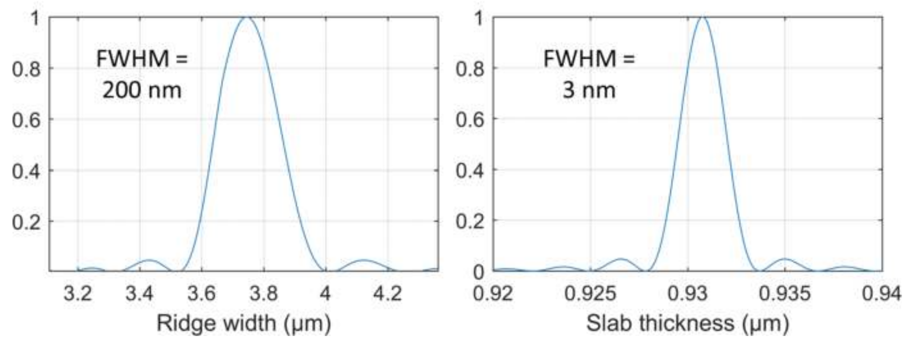

Figure 4.
Normalized SPDC efficiency as a function of ridge width and thickness.

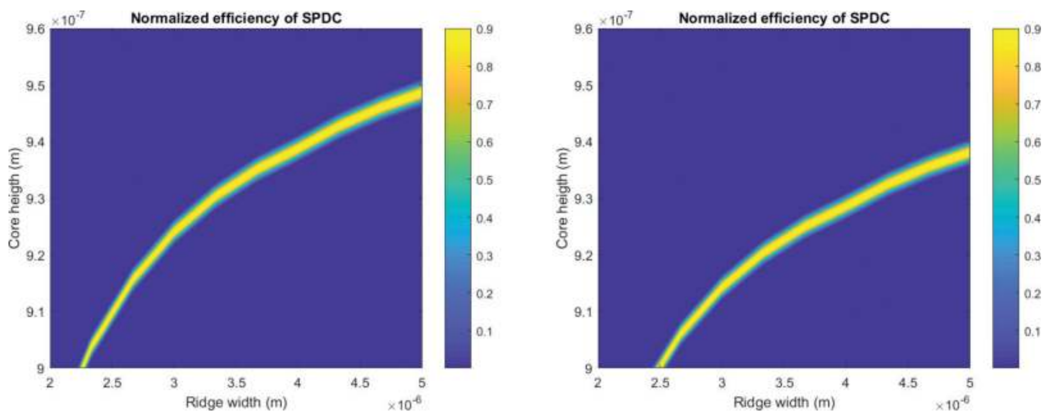

Figure 5.
Normalized SPDC efficiency as a function of ridge width and thickness, for a waveguide temperature of 20°C (left) and 50°C (left). Pump wavelength is 1 μm in both cases.

Fortunately, two tools allow us to shift the efficiency curve: temperature and pump wavelength. **Figure 5** shows the normalized SPDC efficiency as a function of ridge width and thickness, for waveguide temperatures of 20 and 50°C. A temperature shift of 30°C can compensate for a 10-nm variation of the waveguide core thickness. We stress here that the temperatures of laser and parametric conversion regions can be set separately and that an increase of 30°C in the SPDC area has a negligible impact on the laser temperature, assuming that the two regions are separated by 300 μm (a typical distance for adiabatic transfer).

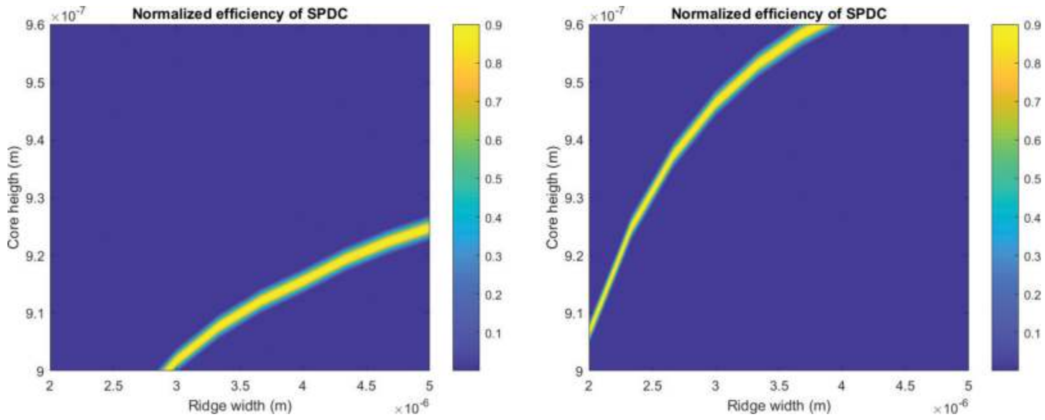

Figure 6.
Normalized SPDC efficiency as a function of ridge width and thickness, for pump wavelengths of 990 nm (left) and 1010 nm (right). Temperature is 20°C in both cases.

Figure 6 presents the normalized spontaneous down-conversion (SPDC) efficiency as a function of ridge width and thickness, at pump wavelengths of 990 and 1010 nm. A wavelength shift of + − 10 nm can compensate for a variation of 40 nm of the waveguide core thickness. This variation is typically accessible to a single-mode DFB laser.

As a conclusion, while efficient parametric down-conversion is only encountered in a narrow window of parameters, it can realistically be achieved by compensating variations in fabrication with a shift in temperature and pump wavelength.

3.3 DBR design

The DBRs should provide a reflectivity above 95% at both signal and idler wavelengths (see **Figure 3**) and nearly null reflectivity at pump wavelength. As mentioned earlier, this has already been demonstrated with dielectric stacks deposited on the waveguide facets [6]. While the outer mirror can be fabricated in this fashion, the inner one needs to be etched at an interface. Let us estimate now the DBR coupling constants in the approximation of weak perturbations. For a DBR length of 100 μm, the coupling constant should be 220 cm^{-1} in order to achieve 95% reflectivity. **Table 4** presents the coupling constants of the fundamental TE and TM modes at 2 μm for a grating depth of 200 nm. The grating is supposed to be perfectly rectangular, with a filling factor of one-half. Whether the grating is formed by etching the top interface (air/GaAs) or by etching the underlying cladding and restarting epitaxy ($GaAs/Al_{0.8}Ga_{0.2}As$ interface), an etch depth of at least 200 nm is necessary to achieve reflectivity over 95% with a DBR smaller than 100 μm.

	Grating at the top interface (air/GaAs)		**Grating at the lower interface ($GaAs/Al_{0.8}Ga_{0.2}As$)**	
Grating depth (nm)	κ_{TE} (cm^{-1})	κ_{TM} (cm^{-1})	κ_{TE} (cm^{-1})	κ_{TM} (cm^{-1})
200	214.5	242.5	277	180.9

Table 4.
Coupling constants for fundamental TE and TM modes at 2 μm, given a rectangular grating of depth 200 nm and duty cycle 50%.

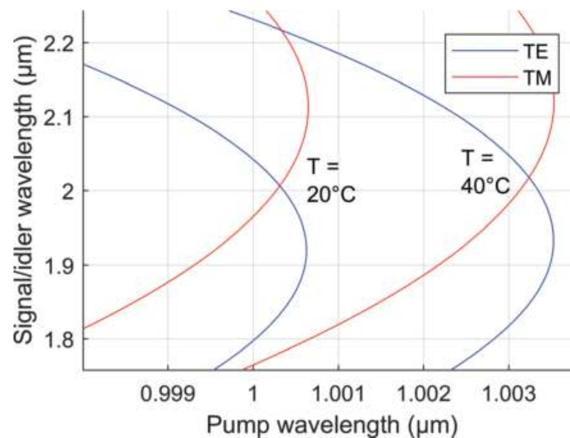

Figure 7.
Tunability curves of the waveguide supporting frequency conversion.

3.4 Tunability

We show in **Figure 7** the tunability curves of the waveguide at temperatures 20 and 40°C. Outside of degeneracy, a signal/idler wavelength range of 300 nm is accessible for a pump wavelength variation of a few nm.

4. Waveguide coupling

4.1 2D approximation for the effective index

A transverse view of the structure is shown in **Figure 8**. The two waveguides are separated by 300 nm of $Al_{0.3}Ga_{0.7}As$. **Figure 9** presents a simulation of light propagation along the structure by a beam propagation method (BPM), which has been carried out with the commercial software RSoft. To reduce calculation time and quickly converge on an intuitive model, we first make a 2D effective-index approximation, whose validity will be checked in the next section. The injected mode, visible on the right-end side of **Figure 9a**, is the eigenmode presenting the highest overlap with the active region. As is visible from **Figure 9b**, 90% of the guided power is contained in the laser core layer at Z = 0, that is, before the taper. Thus, modal gain is expected to not suffer from the presence of the underlying GaAs layer. From Z = 0 to Z = 300 μm, the two top layer widths are reduced from 4 μm to 0. From Z = 300 μm to Z = 500 μm, the separation layer ($Al_{0.3}Ga_{0.7}As$) width is reduced in the same way. Over 95% of the power is transferred to the GaAs waveguide. To estimate the robustness of the design to a limited resolution in lithography, we simulate the same transfer with widths ending at 0.4 μm instead of 0: the transfer of power to the underlying waveguide is 85%. While a more detailed set of tests would be necessary to account for fabrication-induced deviations, these results are encouraging.

In order to find out if the power in the slab is in the desired TE_2 mode, we calculate the overlap of the BPM-simulated field with the GaAs waveguide eigenmodes. The result, reported in **Figure 10**, is that 97% of the power is in the TE_2 mode after one transfer length.

4.2 3D simulations

In the 2D-effective index approximation made in the previous section, we assumed single-mode behavior in the lateral direction. The geometry chosen in 3D

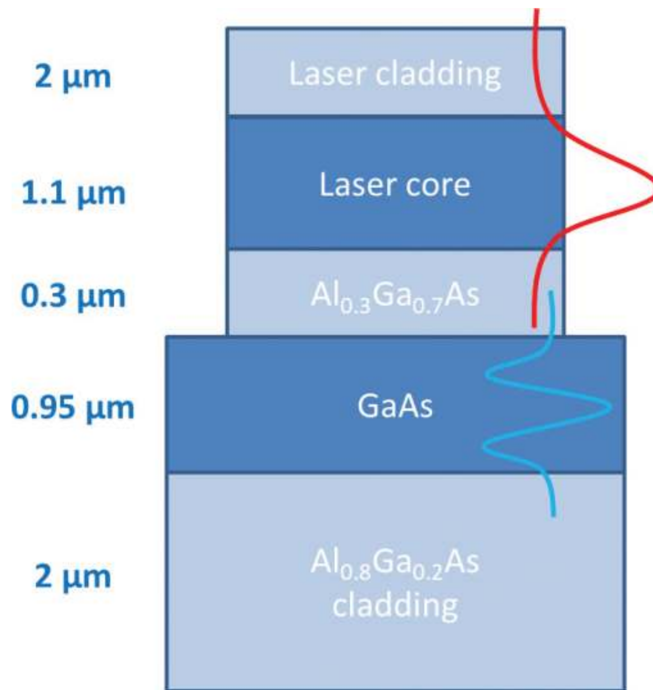

Figure 8.
Transverse view of the structure. The fundamental mode of the top waveguide is shown in blue. Second-order mode of the lower waveguide is shown in red. The three top layers (laser cladding, laser core, and $Al_{0.3}Ga_{0.7}As$ separation) have widths varying from 4 to 0 µm. The GaAs waveguide and inferior cladding have infinite width.

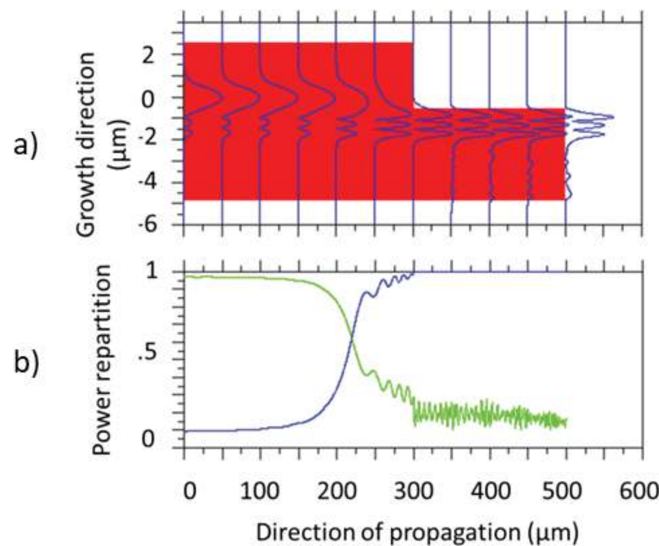

Figure 9.
(a) BPM simulation of light propagation in the structure. (b) Normalized guided power along z, in the upper (laser, blue) and the lower (OPO, green) waveguide.

must balance two conditions in order to give a high transfer to the TE_{20} mode. On the one hand, the lateral confinement of the buried waveguide should be minimal so that the single-mode approximation is satisfied, and coupling to higher order modes in the lateral direction is minimized. On the other hand, the buried waveguide should be confined enough to prevent the field from escaping.

Figure 11 shows the proposed taper design. From Z = 0 to Z = 300 µm, the width of laser cladding, top half of the laser core and QW, is reduced from 4 µm to

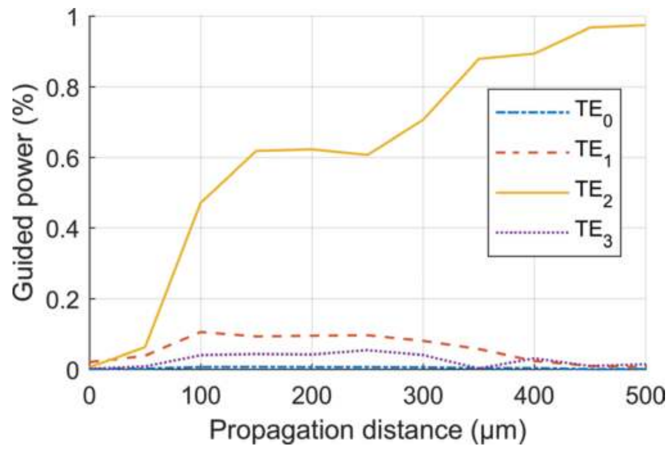

Figure 10.
Modal decomposition of the BPM-simulated field in **Figure 9** *on the eigenmodes of the GaAs waveguide.*

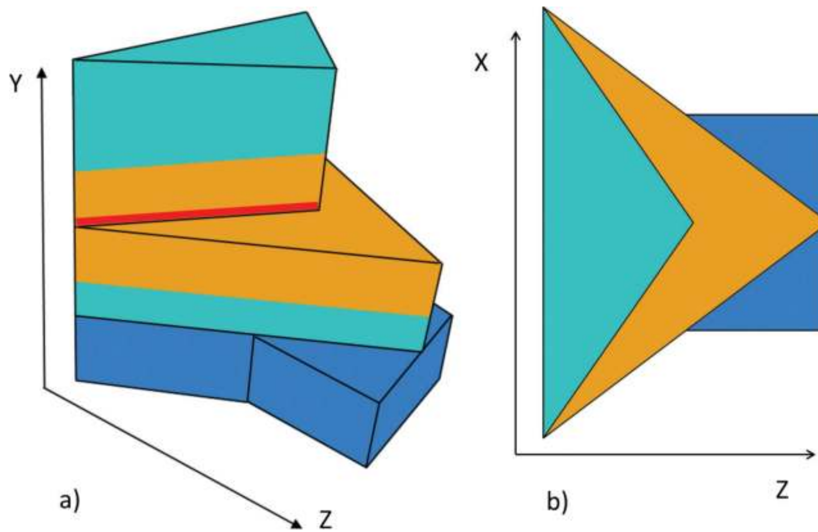

Figure 11.
Side (a) and top (b) view of the proposed taper geometry. Green, $Al_{0.3}Ga_{0.7}As$; orange, laser core layer; dark blue, GaAs; red, quantum well. Dimensions are not to scale.

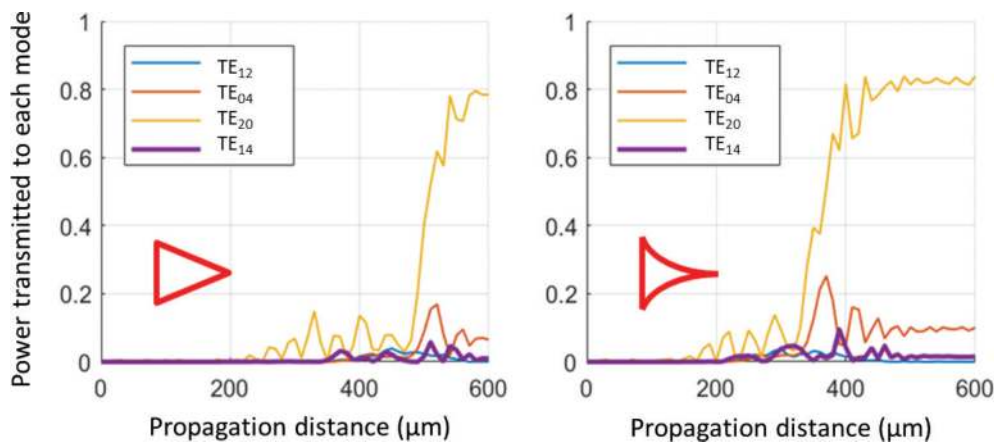

Figure 12.
Power transmitted to the eigenmodes in **Figure 13***. (Left) Triangular tapers. (Right) Quadratic tapers.*

0. From Z = 300 μm to Z = 600 μm, the width of the bottom half of laser core and separation layer ($Al_{0.3}Ga_{0.7}As$) is reduced in the same way. The width of the final GaAs waveguide is 2 μm. For this design, the calculated transfer efficiency into the TE_{20} mode is as large as 80%.

Figure 12 shows the power transmitted to the eigenmodes of the 2 μm wide and air clad GaAs ridge waveguide that are plotted in **Figure 13**. For the sake of clarity, among all the eigenmodes supported by the waveguide, we only show those that are the most likely to sustain a transfer (because they have a similar effective index, the same polarization, and the same horizontal parity as the laser mode).

Modifying the taper shape affects the effective index and thus the position of transfer. A − 0.02 shift in the laser core and cladding refractive indices accelerates the transfer without affecting the total transmission. An opposite shift (+0.02), which can be caused by a 30°C temperature increase, makes the transfer drop to 30–40% depending on the taper shape.

These values must be compared to the estimated OPO thresholds (**Figure 3**): depending on the OPO cavity length and mirror reflectivity, its threshold can range from 20 to 100 mW. Transmission of 30–80% thus sets the target optical power at 25–300 mW. Since AlGaAs laser diodes at 980 nm can emit powers in excess of 10 W in broad area configurations [13] and 700–1500 mW in narrow, laterally single-mode configurations [12], our target power seems within reach.

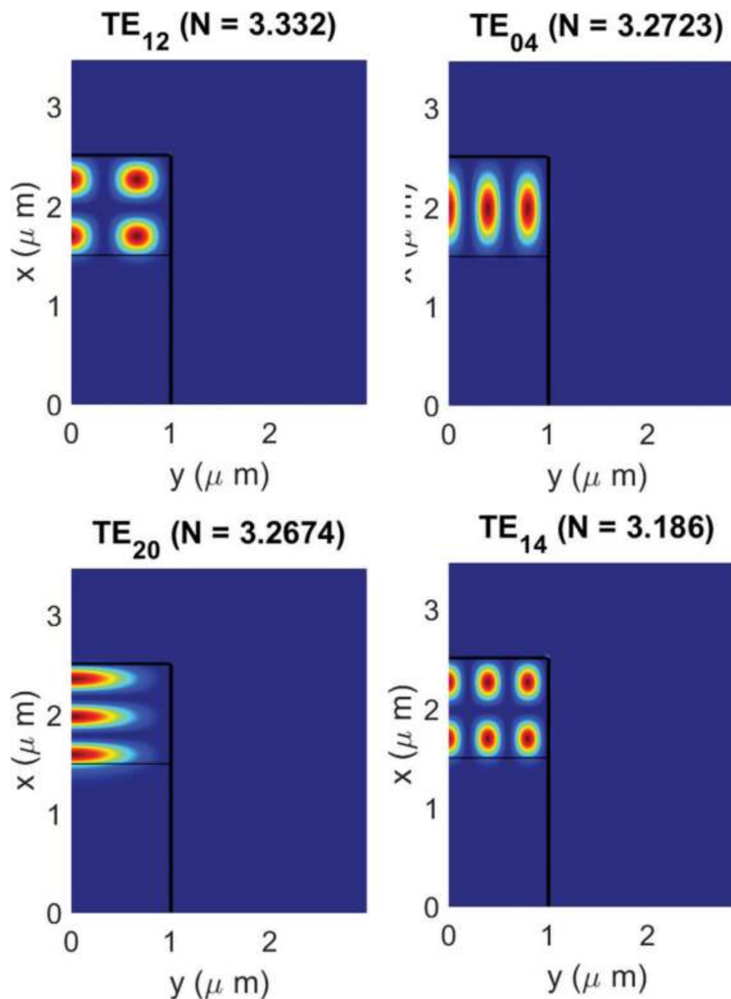

Figure 13.
Four eigenmodes of the ridge GaAs waveguide of width 2 μm. The pump mode for SPDC is TE_{20} (bottom left). Only half of the waveguide is represented in the lateral direction for symmetry reasons.

5. Laser

We propose here a preliminary description of the laser cavity. While the laser design is unconventional, we show that its key parameters (confinement in the QW, reflectivity, estimated differential efficiency) fall in a typical range of values for AlGaAs lasers. Active properties are not investigated, although they could be undertaken in the future on the basis of this work.

5.1 Thermal behavior

As mentioned earlier, thermal behavior is a critical point for the operation of the DOPO source. Given a maximal ridge width for single-mode operation, an epi-up geometry, and a target optical power, we can estimate the temperature rise in the laser.

The laser ridge width is taken to be 5 µm, as this size provides single-mode operation for an index contrast of 0.005 [12]. Assuming a target optical power of 100 mW and a wall-plug efficiency of 16%, the emitted power in the form of heat is 500 mW. We simulate a crude model of the temperature rise with the software COMSOL. The heat is assumed to escape fully from the junction of size 5 µm × 0.1 µm × L (1, 2, or 3 mm) (**Figure 14**). The latter is set inside 10 µm of $Al_{0.3}Ga_{0.7}As$, and the underlying material is GaAs. **Figure 15** shows the junction temperature calculated as a function of the substrate thickness for three different lengths (L = 1, 2, or 3 mm).

To stay under 40°C, we find that the laser should be at least 2 mm long and the wall-plug efficiency should be over 16% at the target power.

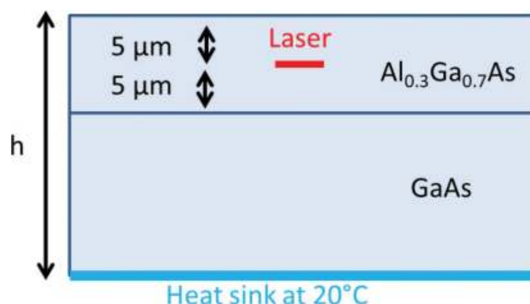

Figure 14.
Model used to estimate the laser temperature rise.

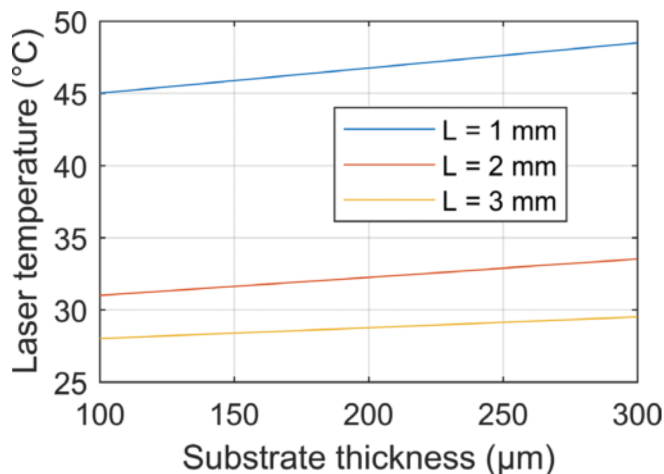

Figure 15.
Junction temperature as a function substrate thickness, for three laser lengths.

5.2 Key parameters

To limit its temperature rise, the laser should be at the least 2 mm long. This size is above the average for common sources in integrated optics, which often favor compactness. Large DFB grating lengths increase modal reflectivity, not only lowering threshold but also degrading differential efficiency. Furthermore, the laser mode is only partially confined before the taper, so we estimate the impact of confinement on the modal gain.

In order to achieve high optical powers and single-mode operation, we propose a DFB laser with low grating reflectivity and high reflectivity (HR) coating on the external facet. We assume that the DFB grating is etched at the interface between laser core and top cladding. To avoid regrowth, gratings can also be etched on the surface [16]. However, optimization of surface gratings depends on the top contact geometry, which has not been defined yet. Therefore, we present only the buried grating case.

If the laser is 1–2 mm long to limit temperature rise, an etch depth of 10–20 nm is necessary to provide a κL product of ~0.5 (where κ is the coupling constant of the fundamental mode). This value is realistically achievable with a shallow etch and epitaxy regrowth.

For a laser of length 2 mm with a coating of reflectivity 90% on the external facet, assuming a κL product of 0.5, total output coupling losses are 9 cm^{-1} [17]. If parasitic losses are 10 cm^{-1} and internal efficiency is 80%, external differential efficiency is 0.38. The modal gain needed to reach laser oscillation is 19 cm^{-1} [17]. QW lasers at 980 nm commonly achieve modal gains in excess of this value [18]; however, the threshold is also affected by the confinement factor. For a single QW of thickness (10 nm), we find that the confinement of lasing mode in the well is 1.2%, which corresponds to a material gain of 1600 cm^{-1} at threshold. This is achieved under a carrier density of 2.5×10^{18} cm^{-3} in the well [19]. Assuming a recombination time of 3 ns, the threshold current density is then expected to be 130 A/cm^2, comparable to the range of 120–150 A/cm^2 measured in similar lasers [13, 18].

In conclusion, we have shown that the key parameters (threshold and efficiency) of this laser are not affected by its unusual design and that they are compatible with operation in excess of 100 mW.

6. Conclusion

We have defined the main conditions required for a diode-OPO structure based on a vertical coupler, and we have described the passive properties of this source. Phase matching can be dynamically controlled through wavelength and temperature tuning. We achieve transfer to a higher order mode of the structure, with sufficient efficiency. The taper layout can still be improved via further optimization.

Overall, this design predicts promising results for the fabrication of an integrated diode-OPO based on GaAs. Unlike all-in-one DOPO configurations, this device does not require record-low propagation losses in the laser diode.

While fabrication of this device is complex, epitaxy regrowth can be avoided completely if the laser DFB grating can be defined at the surface. Most of the technological complexity occurs in the various etching levels necessary to define the structure, from tapers to DFB grating to DBRs.

To ensure feasibility of this project, future work should focus on laser design, particularly on expected optical power and impact of doping on the transfer.

Acknowledgements

This work is supported by a public grant overseen by the French National Research Agency (ANR) as part of the project DOPO. The authors thank the Commissariat à l'Energie Atomique and Direction Générale de l'Armement for the PhD funding. We thank Michel Krakowski and Bruno Gérard for their information and stimulating discussions.

Author details

Alice Bernard[1,2], Jean-Michel Gérard[2], Ivan Favero[1] and Giuseppe Leo[1]*

1 Laboratoire Matériaux et Phénomènes Quantiques, UMR 7162, Université Paris Diderot–CNRS, Paris, France

2 Université Grenoble-Alpes, CEA, INAC-PHELIQS, CEA-CNRS Nanophysics and Semiconductors Joint Group, Grenoble, France

*Address all correspondence to: giuseppe.leo@univ-paris-diderot.fr

© 2018 The Author(s). Licensee IntechOpen. This chapter is distributed under the terms of the Creative Commons Attribution License (http://creativecommons.org/licenses/by/3.0), which permits unrestricted use, distribution, and reproduction in any medium, provided the original work is properly cited.

References

[1] Nathan MI, Dumke WP, Burns G, Dill FH, Lasher G. Stimulated emission of radiation from GaAs p-n junctions. Applied Physics Letters. Nov. 1962;**1**(3):62-64

[2] Hall RN, Fenner GE, Kingsley JD, Soltys TJ, Carlson RO. Coherent light emission from GaAs junctions. Physical Review Letters. Nov. 1962;**9**(9):366-368

[3] Grisard A, Gutty F, Lallier E, Gérard B. Compact fiber laser-pumped mid-infrared source based on orientation-patterned Gallium Arsenide. In: Technologies for Optical Countermeasures VII. Vol. 7836; 2010. p. 783606

[4] Boitier F et al. Electrically injected photon-pair source at room temperature. Physical Review Letters. May 2014;**112**(18):183901-1-183901-5

[5] Oron MB, Blau P, Pearl S, Katz M. Optical parametric oscillation in orientation patterned GaAs waveguides. In: Nonlinear Frequency Generation and Conversion: Materials, Devices, and Applications XI. Vol. 8240; 2012. p. 82400C

[6] Savanier M. et al. Near-infrared optical parametric oscillator in a III-V semiconductor waveguide. Applied Physics Letters. Dec. 2013;**103**(26):261105

[7] Zareian N, Helmy AS. Static and dynamic characteristics of integrated semiconductor optical parametric oscillators. Journal of the Optical Society of America B. Aug. 2013;**30**(8):2306

[8] Andronico A, Gérard JM, Favero I, Ducci S, Leo G. Quantum dot parametric source. Optics Communication. Sep. 2014;**327**:27-30

[9] Fengnian X, Menon VM, Forrest SR. Photonic integration using asymmetric twin-waveguide (ATG) technology: Part I-concepts and theory. IEEE Journal of Selected Topics in Quantum Electronics. Jan. 2005;**11**(1):17-29

[10] Yariv A, Sun X. Supermode Si/III-V hybrid lasers, optical amplifiers and modulators: A proposal and analysis. Optics Express. 2007;**15**(15):9147-9151

[11] Keyvaninia S et al. Demonstration of a heterogeneously integrated III-V/SOI single wavelength tunable laser. Optics Express. Feb. 2013;**21**(3):3784-3792

[12] Wenzel H et al. Fundamental-lateral mode stabilized high-power ridge-waveguide lasers with a low beam divergence. IEEE Photonics Technology Letters. Feb. 2008;**20**(3):214-216

[13] Krakowski M et al. Very high-power broad area laser diode with internal wavelength stabilization at 975 nm for Yb fibre laser pumping. In: Novel In-Plane Semiconductor Lasers XIII. Vol. 9002; 2014. p. 90021G

[14] Beaudoin M, DeVries AJG, Johnson SR, Laman H, Tiedje T. Optical absorption edge of semi-insulating GaAs and InP at high temperatures. Applied Physics Letters. Jun. 1997;**70**(26):3540-3542

[15] Ruan Z, Veronis G, Vodopyanov KL, Fejer MM, Fan S. Enhancement of optics-to-THz conversion efficiency by metallic slot waveguides. Optics Express. 2009;**17**(16):13502-13515

[16] Dridi K, Benhsaien A, Akrout A, Zhang J, Hall T. Narrow-linewidth three-electrode regrowth-free semiconductor DFB lasers with uniform surface grating. In: Novel In-Plane Semiconductor Lasers XII. Vol. 8640;2013. p. 864009

[17] Coldren LA, Corzine SW, Mashanovitch ML. Diode Lasers and Photonic Integrated Circuits. Vol. 218. Hoboken, New Jersey: John Wiley & Sons; 2012

[18] Klopf F, Reithmaier JP, Forchel A. Highly efficient GaInAs/(Al)GaAs quantum-dot lasers based on a single active layer versus 980 nm high-power quantum-well lasers. Applied Physics Letters. Aug. 2000;77(10):1419-1421

[19] Corzine SW, Yan RH, Coldren LA. Theoretical gain in strained InGaAs/AlGaAs quantum wells including valence-band mixing effects. Applied Physics Letters. Dec. 1990;57(26):2835-2837